A Realistic Model for Actively Modelocked Semiconductor Lasers

Liu Zheng, Curtis R. Menyuk and Gary M. Carter

Abstract—**Experiments show that pulses generated by a semiconductor laser modelocked with a frequency limiting element are often not transform limited, indicating the existence of a frequency chirp. A model is developed to calculate the experimentally observed quantities such as the frequency spectrum and the temperal autocorrelation function both before and after pulse compression. The model indicates that the gain nonlinearity plays a crucial role in determining the rate of frequency chirp in the pulse. Good agreement with our experimental data for a single quantum well laser is obtained when the gain nonlinearity is set to $\epsilon_s = 7 \times 10^{-23}$ m^3.**

I. Introduction

Actively modelocked semiconductor lasers with frequency limiting elements are widely used to generate single-mode picosecond pulses. While these pulses are not transform limited due to excess chirp [1], [2], one may use a dispersive time delay line to compensate for the chirp and obtain nearly transform limited pulses. In this paper, we present a theoretical model which describes this excess chirp and predicts the pulse compression. The equations in this model are similar to the traveling wave rate equations [3], [4], but instead of calculating the photon density, we calculate the electric field directly, thus obtaining phase as well as amplitude information, as does the transmission line model [5] and [6]. However, our approach is simpler to implement than the transmission line model, since our approach does not require the development of an equivalent circuit model of the field equations. Our model uses realistic parameters taken or estimated from our modelocking and pulse compression experiments [2]. We find that nonlinear gain has to be added to the model to obtain reasonable agreement with our experimental data. The addition of spontaneous emission noise to the model leads to amplitude and timing jitter in the pulse train. By performing an average over time with a reasonable number of pulses in the train, we obtain excellent agreement with our experimentally determined autocorrelation measurements and optical spectra both before and after pulse compression.

II. Electric Field Traveling Wave Model

The system we are modeling is the same as in [2] — a quantum well laser diode in an external cavity with a grating as the end-reflector/output coupler. Let z be the direction along which light travels from the laser chip to the external cavity. A laser of length L ($0 < z < L$), with its front facet anti-reflection coated and its back facet high-reflection coated and a Littrow mounted grating at $z = L_{\text{ext}} + L$ form an external cavity with a total round trip time T.

Let ε^+ represents the electric field traveling along the z axis, and let ε^- represent the electric field traveling in the opposite direction,

$$\varepsilon^{\pm} = [E^{\pm}(z,t)e^{i(\omega_0 t \mp kz)} + c.c.]/2, \tag{1}$$

where ω_0 is the angular frequency of the optical carrier, k is the wave vector, and $c.c.$ means complex conjugate. The quantities $E^{\pm}$ indicate the slowly varying complex envelopes of the electric field. One can derive the traveling wave electric field model using Maxwell's equations for $\varepsilon^{\pm}$ [7] and the rate equations for the carrier density N [8]. Inside the gain medium, one finds

$$\frac{\partial N}{\partial t} = j(t) - \frac{N}{\tau_n} - g[1 - \epsilon_s P(z,t)] \times (N - N_{\text{tr}})P(z,t), \tag{2}$$

$$\frac{\partial E^+}{\partial z} + \frac{1}{v_g}\frac{\partial E^+}{\partial t} = -\frac{E^+}{2v_g\tau_p} + B[1 - \epsilon_s P(z,t) + i\alpha] \times (N - N_{\text{tr}})E^+ + F_n, \tag{3}$$

$$-\frac{\partial E^-}{\partial z} + \frac{1}{v_g}\frac{\partial E^-}{\partial t} = -\frac{E^-}{2v_g\tau_p} + B[1 - \epsilon_s P(z,t) + i\alpha] \times (N - N_{\text{tr}})E^- + F_n, \tag{4}$$

where N, E^+, and E^- are all functions of z and t. The quantity $P(z,t)$ is the photon density and depends on $E^{\pm}$. The photon lifetime τ_p only includes the laser internal loss caused by free carrier absorption and scattering. Values for the quantities v_g, τ_n, α, g, N_{tr}, ϵ_s, and Γ are shown in Table I, and $B = \Gamma g/2v_g$. The total active modulation current $j(t)$ consists of a sinusoidal current i_{ac} with a period T_{RF} and a DC bias current i_{dc}, as shown in Table I.

The function F_n represents the Langevin contribution due to spontaneous emission noise. In order to include this contribution in our simulations, we add a noise field $\delta E^{\pm}$ with a random phase φ_s to $E^{\pm}$ at each step in the simulation so that the total noise power agrees with the quantum mechanically derived fundamental noise limit [9] [10],

$$\delta E^{\pm} = [4h\nu(e^{\Gamma g N \triangle z/v_g} - 1)/(n^2\epsilon_0 AL)]^{1/2} e^{i\varphi_s}, \tag{5}$$

where $h\nu$ is the photon energy, ϵ_0 is the vacuum electric permeability, n is the effective index of refraction of the laser, $\triangle z$ is the simulation step size, and A is the effective area of the transverse mode.

Manuscript received August 16, 1993; revised November 12, 1993.

The authors are with the Department of Electrical Engineering, University of Maryland Baltimore County, Baltimore, MD 21228.

IEEE Log Number 9216347.

TABLE I
PARAMETER VALUES USED IN THE CALCULATIONS

Variable	Symbol	Value	Unit
Lasing wavelength[a]	λ	0.8	μm
Effective index of refraction[a]	n	4.5	
Carrier lifetime due to spontaneous emission[b][13]	τ_n	1.0×10^{-9}	s
Photon lifetime due to internal loss[b][13]	τ_p	1.0×10^{-9}	s
Carrier density at transparency[a]	N_{tr}	3.0×10^{24}	m^{-3}
Grating bandwidth[a]	f_g	220	GHz
Henry α factor[a]	α	4.0	
Differential gain constant[b][11]	g	2.7×10^{-12}	m^{-3}/s
Gain nonlinearity coefficient[c]	ϵ_s	7×10^{-24}	m^{-3}
Optical confinement factor[b][11]	Γ	0.03	
Factor for leakage current[b][12]	f_{leak}	0.52	
DC bias current[a]	i_{dc}	45	mA
AC peak current[a]	i_{ac}	160	mA
AC current period[c]	T_{RF}	246.5	ps
Total round trip time[a]	T	250	ps
External time	T_{ext}	234	ps
Active region length[a]	L	500	μm
Active region width[a]	W	4	μm
Active region height[a]	H	100	Å
Total external cavity feedback factor[a]	r	0.5	

Note: Superscript a means the parameters are either the same as that used in the experiment, or derived from experimental data; b means the parameters are estimations based on [11], [12], [13]; c means that parameters are determined by fitting experimental data with calculations.

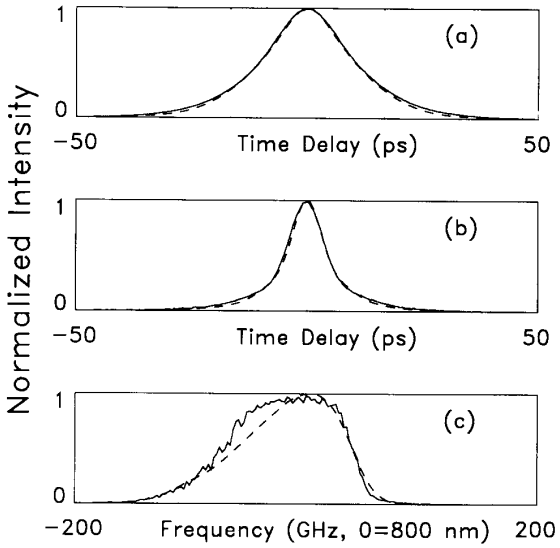

Fig. 1. Solid line—: experimental data. Dashed line - - - - -: calculated results. (a)Autocorrelations of modelocked pulses of a semiconductor laser in an external cavity with a frequency limiting element. (b) Autocorrelations of the pulses shown in (a) compressed by a linear dispersive delay line. (c) The spectra corresponding to the pulses shown in (a) and (b).

The boundary condition at $z = 0$ is $E^+ = E^-$. The boundary condition at $z = L$ includes the time delay and the spectral filtering due to the grating,

$$E^-(z = L, t' = t) = r \times \mathcal{F}[E^+(z = L, t' = t - T_{\text{ext}})], \quad (6)$$

where T_{ext} is the time that the pulse spends outside the laser during one round trip. The function $\mathcal{F}(\cdot)$ represents the filtering, which selects a frequency range limited by the grating bandwidth. Numerically, we take the Fourier transform of the function $E^+(z = L, t' = t - T_{\text{ext}})$, multiply this frequency function by the grating's transfer function, which we assume to be Gaussian, and we then take the inverse Fourier transform of this product to obtain the field in the time domain. The quantity r is the total feedback coupling coefficient, which includes the grating's reflectivity loss and the loss of feedback coupling lens. The equations are solved using variable transformations similar to those described in [7] and with a finite difference scheme. The simulation starts from quantum noise and requires roughly 1000 round trips to reach a quasi-steady-state.

III. RESULTS AND DISCUSSIONS

Table I lists the values of the parameters used in the calculation. In the rest of the paper, all the calculated autocorrelation functions and spectra are averaged over 200 pulses.

Fig. 1 compares our simulation results to the experimental data. All the solid lines are taken from experiments, while all the dashed lines are calculated using our model with the parameters listed in Table I. In particular, we have set $\epsilon_s = 7 \times 10^{-24}$ m^3. Fig. 1(a) shows the autocorrelation results before pulse compression with a FWHM of 22 ps in the experimental data and a FWHM of 21 ps in the calculated results. The corresponding spectra are shown in Fig. 1(c) with a FWHM of 120 GHz for experimental data and 104 GHz for the calculated results. The time-bandwidth products are larger than the transform limit, a result which is mainly caused by the nearly linear frequency chirp. In the experiment, we shortened the modelocked pulses by sending them through a fiber compressor which consisted of 550 meters of single mode optical fiber. We simulated this pulse compression process in our model by imposing a quadratic phase delay on the propagating pulse. The compressed pulse autocorrelation results are shown in Fig. 1(b), with a FWHM of 9.5 ps for the experimental data and 9.0 ps for the theoretical calculations. The quadratic phase delay in the model corresponds to a fiber length of 700 meters with the assumption that the fiber dispersion is 60 ps/nm-km.

The pulse broadening and subsequent pulse compression we observed is due to the gain nonlinearity which slows down the speed of carrier depletion, in turn slowing down the pulse formation. The pulse broadening also leads to a decrease in the chirping rate, the frequency change per unit time. However, the chirp is still nearly linear within the pulse interval, so that a linear positive dispersive delay line can be used to compress the pulse. A larger value of the gain nonlinearity leads to a longer pulse duration and hence a smaller chirp rate, resulting in a longer fiber length needed to compress the pulse. A complete discussion of the physical origin of gain nonlinearity is beyond the scope of this paper. Recent research suggests that carrier spatial hole burning, carrier heating, and carrier transport all play a role [14], [15].

To further illustrate the effect of varying the gain nonlinearity, Fig. 2 compares the experimentally observed autocorrelation measurements and two calculated autocorrelation

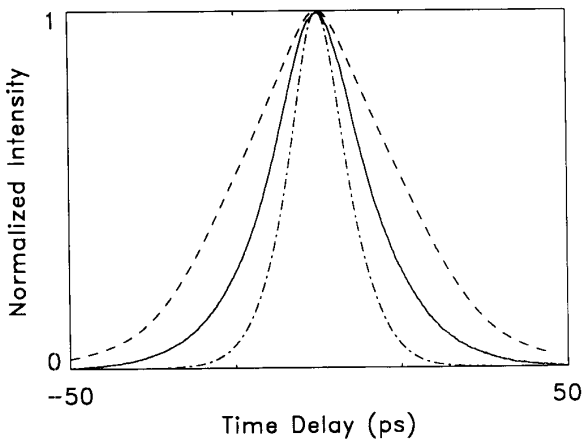

Fig. 2. Autocorrelations of modelocked pulses with different gain nonlinearity factor.Solid line—: experimental data. Dashed line- - - - - : $\epsilon_s = 1.4 \times 10^{-23}$ m^3. Dash-dotted line · — · — ·—: $\epsilon_s = 0$.

functions with the same parameters as in Table I except for the gain nonlinearity factor. The dashed line is calculated with $\epsilon_s = 1.4 \times 10^{-23}$ m^3, double the amount used in Fig. 1, while the dash-dot line is calculated without any gain nonlinearity, $\epsilon_s = 0$. We can see that if there is no gain nonlinearity, the autocorrelation function has a 13 ps width which is smaller than experimentally observed, and with a gain nonlinearity which is too large the calculated autocorrelation function has a width of 36 ps which is wider than observed. The spectral widths in both cases are about the same as that calculated with $\epsilon_s = 7 \times 10^{-24}$ m^3. The compressed pulse autocorrelation functions have widths of 7.5 ps for $\epsilon_s = 0$ and 10.5 ps for $\epsilon_s = 1.4 \times 10^{-23}$ m^3. Only 280 meters of fiber is needed to theoretically compress the pulses with zero gain nonlinearity, while 1100 meters of fiber is needed for pulses with $\epsilon_s = 1.4 \times 10^{-23}$ m^3.

In our model, we use the experimental parameters if possible, and we use reasonable estimates if experimental data are not available. In order to make our modeling results fit the experimental results, we also adjusted the Henry α factor, the grating bandwidth, the differential gain, and the spontaneous emission noise within a reasonable range. However, the inclusion of gain nonlinearity is necessary to make the calculations agree with the experimental data. For our particular laser, Spectra Diode Labs' model SDL-5400-C, the model gives excellent agreement with experimental results when we set $\epsilon_s = 7 \times 10^{-24}$ m^3. Pulses generated in experiments by other researchers [1] have different amount of pulse compression, which we hypothesize is due to the variations of gain nonlinearity in the different lasers.

IV. Conclusion

In conclusion, we have developed a traveling wave electric field model and have used it to simulate an actively modelocked semiconductor laser with a frequency limiting element. We found that we must include the gain nonlinearity to explain the experimentally observed chirp and subsequent pulse compression with a linear dispersive delay line. The gain nonlinearity broadens the pulse, and the nearly linear chirp associated with this broadened pulse makes pulse compression possible by using a linear dispersive delay line.

Dr. Menyuk's work was supported by the Department of Energy. Some of the computational work was carried out at SDSC.

References

[1] J. M. Wiesenfeld, M. Kuznetsov and A. S. Hou, "Tunable, picosecond pulse generation using a compressed, modelocked laser diode source," *IEEE Photonics Tech. Lett.*, vol. 2, pp. 319–321, 1990.

[2] Gary M. Carter and Liu Zheng, "Fiber Compressed high repetition rate pulses from a modelocked GaAs diode laser," *J. Applied Optics*, vol. 32, pp. 4501–4506, 1993.

[3] J. E. Bowers, P. A. Morton, A. Mar and S. W. Corzine, "Actively modelocked semiconductor lasers," *IEEE J. Quantum Electron.*, vol. 25, pp. 1426–1439, 1989.

[4] Paul A. Morton, Roger J. Helkey and John E. Bowers, "Dynamic detuning in actively mode-locked semiconductor lasers," *IEEE J. Quantum Electron.*, vol. 25, pp. 2621–2633, 1989.

[5] Arthur James Lowery, "New dynamic semiconductor laser model based on the transmission-line modelling method," *IEE Proc. J: Optoelectron.*, vol. 134, pp. 281–289, 1987.

[6] A. J. Lowery, "Time-resolved chirp in mode-locked semiconductor lasers," *Electron. Lett.*, vol. 26, pp. 939–940, 1990.

[7] Govind P. Agrawal and N. Anders Olsson, "Self-phase modulation and spectral broadening of optical pulses in semiconductor laser amplifiers," *IEEE J. Quantum Electron.*, vol. 25, pp. 2297–2306, 1989.

[8] Dietrich Marcuse, "Classical derivation of the laser rate equation," *IEEE J. Quantum Electron.*, vol. 19, pp. 1228–1231, 1983.

[9] Dietrich Marcuse, "Computer model of an injection laser amplifier," *IEEE J. Quantum Electron.*, vol. 19, pp. 63–73, 1983.

[10] Klaus Petermann, "Calculated spontaneous emission factor for double-heterostructure injection lasers with gain-induced waveguiding," *J. Quantum Electron.*, vol. 15, pp. 566–570, 1979.

[11] Y. Arakawa and A. Yariv, "Quantum well lasers—gain, spectra, dynamics," *IEEE J. Quantum Electron.*, vol. 22, pp. 1887–1899, 1986.

[12] S. P. Cheng, F. Brillouet and Pascal Correc, "Design of quantum well AlGaAs-GaAs stripe lasers for minimization of threshold current—Applicaion to ridge structures," *IEEE J. Quantum Electron.*, vol. 24, pp. 2433–2440, 1988.

[13] G. P. Agrawal and N. K. Dutta, "Long-wavelength semiconductor lasers," Van Nostrand Reinhold, 1986.

[14] A. Uskov, J. Mork and J. Mark, "Theory of short-pulse gain saturation in semiconductor laser amplifiers," *IEEE Photon. Technol. Lett.*, vol. 4, pp. 443–446, 1992.

[15] Kao-Yang Huang and Gary M. Carter, "Effects of carrier spatial hole burning and structure-dependent nonlinear gain in frequency modelation characteristics of GaAs quantum well external cavity lasers," *LEOS93*, paper number SCL 5.6. November 15–18, 1993, San Jose, California, USA.